Ridge-Bridge Adsorption of Molecular Oxygen on Pt{110}(1 × 2) from First Principles

M. A. Petersen, S. J. Jenkins,* and D. A. King

Department of Chemistry, University of Cambridge, Lensfield Road, Cambridge, CB2 1EW, United Kingdom

Received: December 22, 2005; In Final Form: April 5, 2006

The chemisorption of molecular oxygen on the missing-row reconstructed Pt{110}(1 × 2) surface has been investigated using ab initio calculations based on spin-density functional theory. The calculated energetic, structural, vibrational, and electronic properties of the chemisorbed O_2 species are discussed in terms of the available experimental data. We find that adsorption in the ridge-bridge site is strongly preferred on energetic grounds, relative to adsorption on the {111} microfacets or in the valley sites of the reconstructed surface. We argue in favor of initial adsorption in the ridge-bridge sites, followed by adsorption in the valley long-bridge sites at higher coverages, without excluding the possibility of bridge-site adsorption on the {111} microfacets.

I. Introduction

Recently, there has been an increased interest in characterizing thin surface oxide films formed on transition metal catalysts operating in an oxygen-rich environment.[1−4] An initial step in the formation of such surface oxide films, however, involves the dissociative adsorption of molecular oxygen on the transition metal surface. Such adsorption may be either direct or precursor-mediated and in the latter case may involve either physisorbed or chemisorbed species.

For Pt{110}(1 × 2), which undergoes a missing-row reconstruction giving rise to a hill and valley structure,[5−8] the dissociative adsorption of oxygen is a predominantly precursor-mediated process, in which chemisorbed dioxygen species are thought to play the dominant role.[9] Platinum is a versatile catalyst, used, for example, in automotive catalytic converters for car emission cleanup and for the reforming of petroleum. Platinum has also been demonstrated to be active in methane partial oxidation for conversion of methane to synthesis gas.[10] This has prompted a detailed and extensive molecular beam study of the adsorption, decomposition, and oxidation of methane on the reconstructed Pt{110}(1 × 2) surface,[11−18] in which distinctive roles of chemisorbed dioxygen and atomic oxygen have been suggested.[19]

Although the adsorption of atomic oxygen on Pt{110} has been characterized using scanning tunneling microscopy (STM) and density functional theory (DFT) calculations in recent years,[20] as has the oxidation of Pt{110},[1] studies of molecular oxygen adsorption on Pt{110}(1 × 2) have been restricted to experimental work, predominantly conducted a decade ago. Whether oxygen adsorbs associatively or dissociatively on this surface depends on the substrate temperature. Ohno et al.[21,22] determined on the basis of thermal desorption spectroscopy (TDS) and isotope tracer studies that, at temperatures below 180 K, oxygen adsorbs associatively, with dissociation of the admolecules taking place in the temperature range of 180−220 K. Recombinant desorption of oxygen adatoms was observed above 650 K.

In the low adsorption temperature regime (∼100 K), TDS studies,[21−23] X-ray photoelectron spectroscopy (XPS) results,[24] and work function measurements[23,24] have suggested that more than one type of molecular adspecies can exist on the surface, depending on the coverage. Measurement of the change in work function upon increasing exposure to oxygen showed an initial rapid linear increase followed by a slower rise, with the change occurring at ∼0.6 ML (monolayer) (oxygen atom coverage relative to the surface atom density of the (1 × 1) surface).[23,24] The presence of two regimes was attributed to the sequential adsorption of admolecules in two sites, and Freyer et al.[24] suggested that a bridge site may be occupied first. A saturation coverage of 1.35 ML was determined for molecular adsorption at 120 K.[24] Ohno et al.[21,22] observed three desorption peaks in their TDS spectra with peak temperatures of 200, 180, and 160 K, with the latter two peaks appearing at higher oxygen exposures, further pointing to the presence of multiple species on the surface at higher coverages.

The orientation of the adsorbed dioxygen species has been investigated using angle-resolved photoemission spectroscopy (ARPES)[25] and near-edge X-ray absorption fine structure (NEXAFS) measurements.[22,26] From the ARPES results,[25] it was concluded that at saturation the oxygen admolecules lie parallel to the surface with the internuclear axis orientated in the [1$\bar{1}$0] direction to within ±15°. The NEXAFS study,[22,26] however, distinguished between two different adspecies. In agreement with the ARPES results, a species orientated with the internuclear axis parallel to the bulk surface plane and in the [1$\bar{1}$0] direction was observed. The perpendicular $1\pi_g^*$ orbital of this species was found to be active in the NEXAFS resonances, while the $1\pi_g^*$ orbital orientated parallel to the surface was found to be inactive. [The ground-state electronic configuration of gas-phase O_2 is $[KK](2\sigma_g)^2(2\sigma_u^*)^2(3\sigma_g)^2(1\pi_u)^4(1\pi_g^*)^2(3\sigma_u^*)^0$.] For the second species, the NEXAFS results were consistent with an orientation in which the admolecule is inclined relative to the bulk surface plane. This species was associated with adsorption parallel to the {111} microfacets of the reconstructed Pt{110}(1 × 2) surface. In contrast to the former case, both $1\pi_g^*$ orbitals were suggested to be active for NEXAFS, implying that both of these orbitals remain only partially occupied on adsorption. The alignment of the internuclear axis relative to the {111} facet could not be determined conclusively.

* To whom correspondence should be addressed. E-mail: sjj24@cus.cam.ac.uk.

10.1021/jp057447k CCC: $33.50
Published on Web 06/02/2006

The sites for molecular oxygen adsorption on Pt{110}(1 × 2) have been studied using photoemission from coadsorbed xenon (PAX)[23,27] and surface core-level shift measurements.[28] In both approaches, it was concluded that oxygen adsorption takes place preferentially in the valley sites on the reconstructed Pt{110}(1 × 2) surface, followed by adsorption on the facets at higher coverages.[23] However, the adsorption site identification was based on the results of an ultraviolet photoemission spectroscopy (UPS) study of xenon adsorption on Pt{110}(1 × 2),[29] in which it was *assumed* that xenon adsorption takes place in the valley sites. Interestingly, in a recent theoretical study of Xe adsorption on Pt{111},[30] it was established that Xe preferentially occupies the atop site and not the high-coordination 3-fold sites as generally assumed. This result thus calls into question the assumption that on Pt{110}(1 × 2) Xe would occupy the higher coordination valley sites. In a separate angle-resolved TDS study, Ohno et al.[22] observed that the desorption flux due to oxygen admolecules obeys a simple cosine distribution. This suggests that if the admolecules are adsorbed in valley sites, then the declining terraces of the {111} microfacets should not hinder the translational motion of the molecules as they desorb. This result may equally well point to desorption from adsorption sites on the ridge atoms of the reconstructed Pt{110}(1 × 2) surface, further indicating that the assumption of valley site adsorption may not necessarily be valid.

Electron energy loss spectroscopy (EELS) measurements have been discussed in terms of peroxo-like (O_2^{2-}) and superoxo-like (O_2^-) species adsorbed on the surface.[31,32] Two losses were observed at 860 [31,32] and 930 cm^{-1},[32] with the latter emerging at higher oxygen exposures. These loss peaks were assigned to the O−O stretching frequency of a peroxo-like species adsorbed in a bridge and an atop site, respectively. With increasing oxygen exposure, additional losses at 1250 and 1550 cm^{-1} were observed, which were attributed to chemisorbed superoxo-like species and physisorbed oxygen, respectively. In the former case, the superoxo species was found to desorb below 100 K.

It is worth noting here that the assignment of the loss peaks as due to peroxo-like species was based on measurements of the O−O stretching frequency of peroxo and superoxo species observed in dioxygen metal complexes.[33] The EELS results for O_2 adsorption on Pt{111} were thus also initially interpreted in terms of two peroxo-like species adsorbed on the surface, with corresponding losses observed at 710 and 875 cm^{-1}.[34,35] However, subsequent NEXAFS results for Pt{111} were discussed in terms of a superoxo species,[36,37] and Puglia et al.[38] then later distinguished both superoxo and peroxo chemisorbed molecular phases coadsorbed on Pt{111}. However, in the NEXAFS work, the superoxo and peroxo classification was based on the observed perturbation of one or both of the molecular $1\pi_g^*$ orbitals upon formation of the adsorbate−metal bond, as well as on the O−O bond length as derived from the observed σ^* resonances. The resulting assignment was essentially inconsistent with the classification based solely on the observed stretching frequencies of the same species. In fact, Outka et al.[36] noted that the O−O stretching frequency for superoxo and peroxo species on metal surfaces may be shifted relative to those observed in dioxygen metal complexes.

The observation of two types of chemisorbed species on Pt{111}[38] was subsequently corroborated by a DFT study of O_2 adsorption on Pt{111},[39,40] in which both peroxo-like and superoxo-like chemisorbed molecular species were identified using a classification scheme consistent with that of the NEXAFS approach. The O−O stretching frequency for the superoxo-like species could furthermore be calculated and was found to be 850 cm^{-1}, within the range attributed to peroxo-like species based on the EELS analysis. This would seem to indicate that the EELS results for O_2 adsorption on Pt{110}(1 × 2) are similarly consistent with superoxo species. Panas et al.[41] have further suggested that a superoxo species predominates on this surface, based on their reinterpretation of the ARPES results of Prince et al.[25] for which the positions of the $2\sigma_g$ and $2\sigma_u^*$ resonances were used to classify the type of species present.

As a final point, we note that the adsorption of molecular oxygen on the Pt{110}(1 × 2) surface does not appear to induce the lifting of this reconstruction.[9,42,43] Furthermore, no evidence for the formation of ordered adsorbate structures due to molecular oxygen adsorption at low temperatures on the Pt{110}(1 × 2) surface has been observed.[28,43]

In this paper, we use state of the art DFT calculations to determine the adsorption site preference for O_2 on Pt{110}(1 × 2). We examine the calculated electronic, magnetic, and geometric structure of the most stable species and relate the results to those of the extensive experimental studies on this system, as described above.

II. Calculation Methodology

Total energy periodic slab calculations were performed within the framework of spin-DFT using the CASTEP code.[44] The electronic wave functions were expanded in terms of a plane wave basis set up to a kinetic energy cutoff of 380 eV. The electronic exchange-correlation energy was described using the Perdew−Wang (PW91) form[45] of the generalized gradient approximation (GGA). The electron−ion interactions were included through the use of ultrasoft pseudopotentials[46] on Pt and oxygen, as provided within the CASTEP distribution. A total of 10 valence electrons on each Pt atom and 6 valence electrons on each oxygen atom were thus explicitly treated within the calculations, while the influence of the core electrons was treated implicitly through their contribution to the form of the pseudopotentials.

The calculations were performed using a supercell of length equivalent to 14 layers of Pt in the surface normal direction. A slab consisting of 6 layers of Pt was used to represent the Pt{110} surface, within a (2 × 2) surface unit cell. The vacuum region between the slabs was equivalent to 8 layers of Pt, ∼11 Å, to minimize spurious interactions between neighboring slabs. The dimensions of the supercell were consistent with a conventional lattice parameter of 3.97 Å, as calculated using the GGA (experimental value 3.9236 Å[47]). Brillouin zone integration was achieved by summation over a 5 × 4 × 1 Monkhorst−Pack mesh[48] of special k-points. A Fermi-surface smearing of 0.2 eV was employed in the calculations, and the results were extrapolated to 0 K.[49,50] In terms of the k-points sampling density, kinetic energy cutoff, supercell dimensions, and slab thickness, the above calculation regime proved to be reliable in a series of related calculations for methane decomposition on this surface.[51−53] Calculation of the isolated O_2 molecule gave a binding energy (excluding the zero-point energy) and bond length of 5.71 eV and 1.23 Å, respectively, as compared with the experimental values of 5.17 eV and 1.2074 Å.[47]

The structural optimization calculations were performed with the oxygen molecules placed on one side of the slab, and the adsorbate and the top four Pt layers were allowed to relax under the influence of the calculated Hellmann−Feynman forces. With one O_2 molecule in the (2 × 2) surface unit cell, the coverage

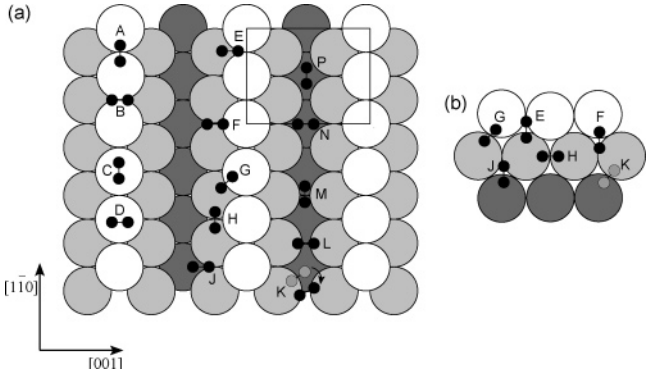

Figure 1. Schematic depiction of sites considered for the chemisorption of molecular oxygen on Pt{110}(1 × 2): (a) top view of the {110} surface and (b) top view of sites on the {111} microfacet; white, light, and dark gray circles represent first-, second- and third-layer Pt atoms, respectively, with oxygen molecules indicated as black dumbbells. The two geometries for site K show the starting configuration (gray) and the final relaxed configuration (black) to which the molecule moves, as described in the text. The (2 × 2) surface unit cell is indicated in the top right corner of (a).

of oxygen molecules corresponds to 0.25 ML, or 0.5 ML in terms of the oxygen atom coverage. All coverages are quoted relative to the surface-layer Pt atom density of the unreconstructed (1 × 1) surface. Due to the computationally demanding nature of the calculations, spin-unpolarized calculations were initially performed for each of the adsorption sites. The calculations were then repeated only for the most stable adsorption sites, using spin-polarization. We note that the adsorption energies for O_2 on Pt{110}(1 × 2) that we report exclude zero-point energy (ZPE) corrections. Test calculations for the six lowest-energy adsorption sites indicate that the ZPE correction for each site is of the order of 0.14−0.15 eV/molecule. The variation in ZPE from one site to another, however, is only of the order of 0.01 eV, and hence ZPE corrections are not expected to alter the relative energy difference between adsorption sites reported in this paper. Furthermore, we calculate the ZPE of gas-phase O_2 as 0.10 eV, so the net effect of ZPE on our uncorrected adsorption heats will simply be to decrease them by around 0.04−0.05 eV/molecule.

Atom-resolved charges have been obtained using the Bader topological method,[54,55] in which the valence electron density is partitioned into regions attributable to each atom on the basis of topological features of the density distribution. This technique has been shown to be reliable and informative in a number of previous studies.[56−63]

III. Energetics of O_2 Adsorption on Pt{110}(1 × 2)

The clean Pt{110}(1 × 2) surface exhibits a reconstruction of the missing-row form, in which every alternate close-packed row aligned along the [1$\bar{1}$0] direction is absent.[5−8] The reconstruction leads to a highly corrugated surface, consisting of a series of alternating ridges and troughs. The troughs, formed by the missing rows, are bound on either side by {111} microfacets.

The adsorption sites considered in this study are illustrated schematically in Figure 1. Two orientations were considered for the sites located on the ridges (sites A−D) and in the troughs (sites L−P), with the internuclear axis orientated either in the [1$\bar{1}$0] direction along the close-packed rows or in the [001] direction. A further six adsorption sites were considered (sites E−K), corresponding to adsorption on the {111} microfacets (Figure 1b).

TABLE 1: Comparison of the Total Energy per (2 × 2) Cell for O_2 Adsorption on Pt{110}(1 × 2)[a]

site	relative energy (eV)	site	relative energy (eV)
A	0.00	D	1.24
E	0.54	B	1.29
K	0.59	P	1.30
G	0.62	N	1.36
L	0.76	C	1.64
H	0.80	M	2.45
F	0.86	J	unstable

[a] Energies are quoted relative to adsorption in the ridge-bridge site (A), for which an adsorption energy of −1.45 eV/molecule is calculated. Results are for spin-unpolarized calculations.

The results of the spin-unpolarized calculations are summarized in Table 1, in which the total energy is given for each adsorption site relative to that obtained for the lowest-energy site, the bridge site orientated along the Pt ridge (A). Adsorption in site J was found to be unstable, with the oxygen molecule moving from the face-centered cubic (fcc) site at the bottom of the {111} microfacet (site J) into the 4-fold hollow site in the trough (site N).

On the basis of the results of the spin-unpolarized calculations presented in Table 1, the six lowest-energy adsorption sites were investigated further using spin-polarized density functional theory. It is worth noting that five of these sites correspond to adsorption in a 2-fold bridge site (A, G, H, K, L), with the sixth representing adsorption over the fcc site on the {111} microfacet, site E. The chemisorption energies, E_{ads}, calculated for each site with reference to the clean Pt{110}(1 × 2) slab and the gas-phase O_2 molecule, $E_{ads} = E_{total} - E_{clean} - E_{O_2}$, are summarized in Table 2. We note that the starting configuration with the O_2 molecule placed in the bridge site at the bottom of the {111} facet (site K) resulted in the molecule drifting into the neighboring long-bridge site with the internuclear axis rotated 27.2 ° relative to the [001] direction. This configuration differs from the ideal long-bridge adsorption along the [001] direction by 0.05 eV/molecule, with the rotated configuration being slightly more stable. However, for the optimization of the adsorbate structure in the ideal long-bridge site (site L), symmetry constraints were imposed so that a symmetry-breaking rotation of the molecule about the surface normal was disallowed. Vibrational analysis coupled with symmetry-broken test calculations nevertheless indicate that all six lowest-energy sites are true local energy minima, although for site A we note that the potential energy surface is very flat with respect to displacement of the molecule in the [001] direction.

The lowest-energy adsorption site is the bridge site on the ridge (site A), with the internuclear axis of the O_2 molecule orientated in the [1$\bar{1}$0] direction along the close-packed rows. The corresponding adsorption energy is −1.48 eV/molecule. For O_2 adsorption on Pt{110}(1 × 1), Panchenko et al.[64] calculated an adsorption energy of −1.58 eV/molecule for adsorption in the short-bridge site along the close-packed ridge, which was similarly found to be the most stable site on the unreconstructed surface. The adsorption energies calculated for adsorption on the Pt{110} surfaces are thus significantly greater than those found for O_2 adsorption in the bridge site on the Pt{111} surface, for which adsorption energies of −0.85 eV/molecule[39,40] and −0.64 eV/molecule[65] were obtained from periodic slab calculations with ultrasoft pseudopotentials, the PW91[45] functional, and including substrate relaxations. (The small difference between the latter two values for adsorption on the Pt{111} surface, which were obtained using the same computational code, was attributed by Bocquet et al.[65] to

TABLE 2: Calculated Properties of Molecular Oxygen on Pt{110}(1 × 2)[a]

site	description	internuclear axis orientation	E_{ads} (eV/O_2)	d_{O-O} (Å)	z (Å)	ν_{O-O} (cm^{-1})
A	first-layer bridge site	$[1\bar{1}0]$	−1.48	1.36	1.89	877
E	fcc site on {111} microfacet	[001]	−0.92	1.41	1.73	752
G	bridge site between first and second layer	[101]	−0.91	1.35	1.92	882
K	rotated long-bridge site	27.2° relative to [001]	−0.89	1.32	1.62	904
L	long-bridge site	[001]	−0.84	1.32	1.71	944
H	second-layer bridge site	$[1\bar{1}0]$	−0.72	1.35	1.92	886

[a] All properties have been determined using spin-polarized DFT. E_{ads} is the chemisorption energy per O_2 molecule, d_{O-O} is the O−O bond length, z is the "height" of the center of mass of the molecule measured normal to the local surface plane, and ν_{O-O} is the O−O stretching frequency.

nonequivalent calculation conditions, for example, k-point sampling, energy cutoff, unit cell size.)

The higher adsorption energy found for the ridge-bridge site on Pt{110}(1 × 2) compared with bridge-site adsorption on Pt{111} may crudely be rationalized by considering the nearest-neighbor coordination of the surface Pt atoms involved in the adsorbate bond on the two surfaces. For the Pt{110}(1 × 2) surface, the first (ridge), second (microfacet), and third (trough) layer atoms have a coordination of 7, 9, and 11 respectively, while on the Pt{111} surface the coordination number is 9 for all surface atoms. If a low coordination number may be equated with a propensity for stronger binding on adsorption, then the higher chemisorption energy found for adsorption in the ridge-bridge site on Pt{110}(1 × 2) is reasonable, since in this case only the 7-fold coordinated ridge Pt atoms are directly involved. If adsorption in the bridge site on the second layer (site H) is considered instead (in which case the Pt atoms have the same coordination as that of the {111} surface), then the corresponding chemisorption energy of −0.72 eV/molecule is indeed similar to that calculated for adsorption in the bridge site on the {111} surface.[39,40,65] Certainly, this rationalization of the binding energies is crude, as the complex rehybridization and orbital mixing effects which take place on surface−adsorbate bond formation have been neglected. However, consideration of the surface atom coordination does explain the general trend in chemisorption energy observed for similar sites on Pt{110}-(1 × 2) and Pt{111}.

Fusy et al.[23] determined the activation energy for desorption of oxygen from the molecular state on the Pt{110}(1 × 2) surface from their TDS results. For the desorption peaks observed at approximately 180 and 200 K, desorption activation energies of 45 kJ mol^{-1} (0.47 eV/molecule) and 51 kJ mol^{-1} (0.53 eV/molecule) were estimated, respectively. Thus, it would appear at first sight that the low-temperature peaks cannot represent desorption from the ridge-bridge site, with its comparatively high adsorption energy of −1.48 eV/molecule. However, in their TDS work, Fusy et al.[23] reported that desorption from the molecular state was only observed for oxygen coverages above 0.31 ML. At lower coverages, recombinative desorption from the atomic state was observed at temperatures above 650 K. Ohno et al.[21] made a similar observation in their independent TDS work, and Freyer et al.[24] noted in their XPS study that, for preadsorbed molecular oxygen coverages of up to 0.45 ML prepared at 120 K, complete conversion to atomic oxygen occurred upon heating to room temperature. Only at higher coverages was heating accompanied by desorption from the molecular state.

Thus, there are two possible explanations for the observed desorption spectra. The first is that the low-temperature desorption peaks correspond to desorption from the less stable adsorption sites on the {111} microfacets or in the trough (Table 2). In this picture, adsorption in the ridge-bridge site results in dissociation, with adsorption in the less stable sites populated at higher coverages resulting in the emergence of molecular desorption peaks at temperatures of 200 K and below. However, Ohno et al.[21] concluded from the results of their isotope tracer and TDS studies that the low-temperature TDS peak observed at 200 K can be attributed to competitive desorption from the molecular state through which dissociation to atomic oxygen proceeds. It would therefore appear that a second explanation is necessary.

From both EELS[31,32] and XPS[24] studies, it is apparent that the possibility of atomic oxygen coadsorbed with molecular species cannot be excluded even at substrate temperatures as low as 120 K. This was demonstrated by heating a surface preadsorbed with oxygen at low temperatures and observing the evolution of the EELS spectra.[31,32] Already at 125 K, a loss peak attributed to the Pt−O vibration of atomic oxygen was observed. Thus, even at these temperatures, the effect of atomic oxygen coadsorbed on the surface must be taken into account. Since the influence of coadsorbed atomic oxygen on the adsorption energy of molecular oxygen is not considered in our density functional calculations, the chemisorption energies reported in Table 2 cannot be compared directly with the adsorption energies estimated by Fusy et al.[23] Indeed, TDS experiments for O_2 adsorption on Pt{111} have shown that the heat of adsorption for molecular oxygen is reduced from 37 kJ mol^{-1} (0.38 eV/molecule) on the clean Pt{111} surface to about 16 kJ mol^{-1} (0.17 eV/molecule) in the presence of a coadsorbed O(2 × 2) layer.[34] Furthermore, with increasing coverage on Pt-{110}(1 × 2), additional sites will be occupied by molecular oxygen, further influencing the adsorption energies calculated. We note also that the overbinding tendency of the local spin-density approximation, which may not be completely cured by the GGA, may further contribute to an over-estimation of the calculated chemisorption energies, as reported in Table 2. We suggest, therefore, that the 200 K desorption peak may indeed be attributed to desorption from the ridge-bridge site in accord with the analysis of Ohno et al.,[21] provided that the presence of coadsorbed atomic oxygen and, at higher coverages, molecular adspecies leads to a sufficient lowering of the adsorption energy to enable desorption with a peak temperature of 200 K.

The calculated O−O stretching frequencies obtained within the harmonic approximation for each of the most stable adsorbed species are given in Table 2. The three bridge-bonded species aligned along the close-packed ridge (site A), between the first and second layer (site G) and over the second-layer Pt atoms on the {111} facet (site H), all yield similar frequencies of 877, 882, and 886 cm^{-1}, respectively, and are consistent with the calculated vibrational frequency of 850 cm^{-1} for bridge-site adsorption on Pt{111}.[39,40] For the bridge-fcc-top site on the {111} microfacet (site E), a lower frequency of 752 cm^{-1} was obtained, as compared with a frequency of 690 cm^{-1} for a similar site on Pt{111}.[39,40] Adsorption in the long-bridge site of the trough is characterized by slightly higher frequencies for both the rotated (site K) and [001]-aligned (site L) species (904

and 944 cm^{-1}, respectively). The EELS results[31,32] yield a loss peak at ~800 cm^{-1} shifting to 860 cm^{-1} with increasing exposure. At higher coverages, a second loss evolves at 920 cm^{-1} which shifts to 930 cm^{-1} with increasing exposure. Comparison with the calculated stretching frequencies suggests that the low-frequency loss is consistent with the bridge-bonded species, while the higher frequency loss is consistent with adsorption in the long-bridge site. Although it is preferable to consider the shifts in the calculated O−O stretching frequencies relative to that calculated for the gas-phase O_2 molecule, for which we obtain 1615 cm^{-1} (experimental frequency, 1575 cm^{-1}),[47] our calculated frequencies suggest that the fcc site on the {111} microfacet is not populated under the experimental conditions at which the EELS spectra were obtained.

Both NEXAFS [22,26] and ARPES [25] identified a species aligned in the [1$\bar{1}$0] direction and lying parallel to the bulk surface plane of Pt{110}(1 × 2). Furthermore, the NEXAFS study was able to relate this species to the TDS peak observed at 200 K.[21] The identification of the ridge-bridge site (A) as the most stable adsorption site, based on the current calculations, is consistent with this empirical observation, since for adsorption in this site the internuclear axis is indeed orientated along the close-packed rows in the [1$\bar{1}$0] direction and parallel to the bulk surface plane. The remaining adsorption sites which are consistent with the NEXAFS and ARPES results (sites C, H, P, and M in Figure 1) are all strongly disfavored on energetic grounds (Tables 1 and 2) relative to adsorption in the ridge-bridge site.

The NEXAFS results[22,26] further suggest that the oxygen species which desorb below 200 K are inclined relative to the bulk surface plane. This was interpreted in terms of adsorption on the {111} microfacet, although the orientation of the molecular axis with respect to the microfacet could not be determined conclusively. Possible candidates for adsorption on the {111} facet are species E, G, and H (Table 2). Since adsorption in the bridge-fcc-top configuration (site E) can be eliminated on the grounds of the frequency analysis, adsorption in the remaining two bridge sites (G and H) seems probable and is not inconsistent with the frequency results. Nevertheless, the effect of coadsorbed atomic and molecular oxygen on the adsorbate site preference will affect which sites are actually occupied at higher coverages, owing to the effects of lateral interactions between coadsorbed species and competition for bonding to the same substrate atoms at higher coverages.

We note that the PAX results[23,27] were interpreted in terms of adsorption along the valleys (troughs) of the reconstructed surface, followed by adsorption on the {111} facets, while the adsorbate-induced surface core-level shift measurements were similarly attributed to adsorption of oxygen in the troughs.[28] Our DFT results suggest that the most stable adsorption site is in fact located on the ridge atoms. At higher coverages, the EELS results, in combination with our DFT calculations, suggest that the long-bridge site in the valley is occupied, albeit without fully excluding the possibility of adsorption in the bridge sites located on the {111} microfacets. This interpretation is distinct from that put forward by previous authors, in which it was assumed that molecular oxygen first adsorbs at the bottom of the valleys with the molecular axis aligned in the [1$\bar{1}$0] direction along the close-packed rows, followed by adsorption on the facets.

IV. Structural Characterization of Adsorbates

The relaxed structure of O_2 adsorbed in the lowest-energy bridge site on the ridge of the reconstructed Pt{110}(1 × 2) surface is schematically illustrated in Figure 2. The O−O bond

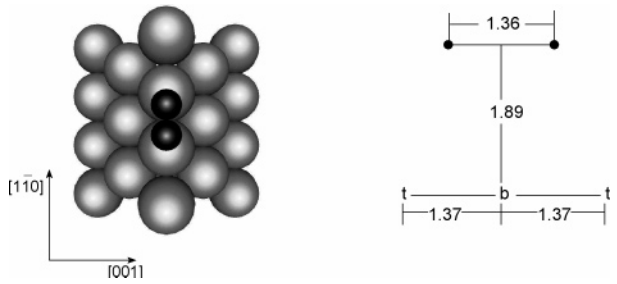

Figure 2. Adsorption geometry of O_2 in the ridge-bridge site (A) on Pt{110}(1 × 2). The adsorption site is illustrated on the left, with the corresponding structure on the right. All distances are in angstroms, with the labels t and b referring to atop and bridge positions, respectively, along the close-packed ridge row.

length is elongated to 1.36 Å upon adsorption, compared with the calculated gas-phase bond length of 1.23 Å. The molecular axis lies parallel to the macroscopic {110} surface plane at a height of 1.89 Å above the first-layer ridge atoms. The resulting O−Pt distance is 2.01 Å. The contraction of the first interlayer spacing of the surface relative to the bulk spacing is reduced from −15.2% for the clean surface (calculated with the same methodology described in section 2) to −8.2% upon adsorption of oxygen, which corresponds to a net vertical displacement of the Pt atoms by 0.10 Å. The first-layer atoms are raised by 0.06 Å, and the second-layer atoms lowered by 0.04 Å relative to the clean surface. The net buckling of the third-layer atoms is reduced from 0.28 Å for the clean surface to 0.20 Å in the presence of O_2. O_2 adsorption therefore partially reverses the lateral and vertical displacements observed for the clean surface, as expected. (For a discussion of the calculated clean Pt{110}-(1 × 2) surface relaxations, refer to ref 8.)

The adsorbate structure is very similar to that calculated for bridge-site adsorption on Pt{111}, for which an O−O bond length of 1.39 Å[39,40] or 1.35 Å[65] was obtained, with the oxygen molecule located at a height of 1.92 Å above the surface.[39,40,65] The similarity of the calculated bond lengths for the two surfaces supports the conjecture of Ohno et al.,[22] based on their NEXAFS results, that the internuclear bond length of O_2 adsorbed on Pt-{110}(1 × 2) approximates that on Pt{111}.

The adsorbate structure at each of the two bridge sites G and H on the {111} microfacet is similar to that of the ridge-bridge site described above. For these two sites, the corresponding O−O bond length is 1.35 Å, with the molecule approximately parallel to the local surface plane of the {111} microfacet at a height of 1.92 Å measured along the microfacet normal. When the chemisorption energies in Table 2 for equivalent bridge sites on the first (A) and second (H) surface layers are compared, it may be noted that a reduction in the adsorption energy of 0.76 eV/molecule is accompanied by only minor changes in the adsorbate geometry. A difference of only 0.01 Å in the bond length and 0.03 Å for the adsorbate height above the respective microscopic surface plane is observed for the ridge and second-layer bridge sites. This suggests that the variation in binding energy for the different bridge sites originates largely from the variation in substrate stabilization upon adsorption at different sites.

For the two orientations at the long-bridge site (K and L), the corresponding O−O bond length is 1.32 Å with an O−Pt bond distance of 2.07 Å. In the rotated configuration (K) illustrated in Figure 3, the molecule lies parallel to the macroscopic {110} plane and is rotated about the surface normal through an angle of 27.2° relative to the [001] direction. The rotated molecule is located at a height of 1.62 Å above the second layer atoms, as opposed to the species aligned in the

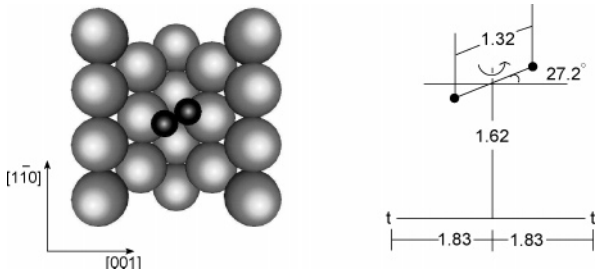

Figure 3. Adsorption geometry of O_2 in the rotated long-bridge site (K), illustrated on the left, on Pt{110}(1 × 2). The relaxed structure on the right indicates the rotation of the molecule about the macroscopic surface normal. All distances are given in angstroms, with the label t referring to the atop position over the second-layer Pt atoms.

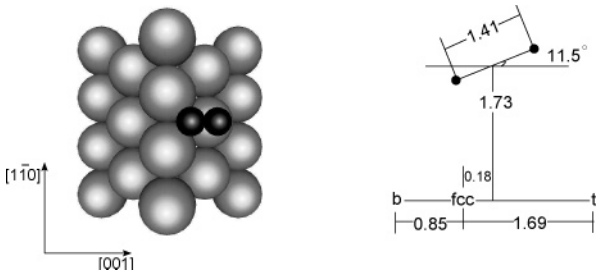

Figure 4. Adsorption geometry for O_2 in the fcc site (E) on Pt{110}-(1 × 2). The schematic illustration of the relaxed structure on the right is orientated relative to the plane of the {111} microfacet. All distances are given in angstroms, with the labels b, fcc, and t referring to bridge, fcc hollow, and atop positions on the {111} microfacet, respectively.

[001] direction, for which the corresponding distance is 1.71 Å. In both cases, the second-layer Pt atoms to which the molecule is bonded each undergo a substantial pairing displacement of ∼0.15 Å toward the missing row. In the rotated configuration, these atoms are raised by 0.19 Å relative to the bare second-layer atoms but only by 0.13 Å in the [001]-aligned geometry. The buckling of the third-layer Pt atoms is reduced from 0.28 Å for the clean surface to 0.17 Å for the adsorbate-covered surface for both adsorbate geometries. The rotated configuration found for O_2 adsorption in the long-bridge site is similar to that calculated for O_2 adsorption on Pt clusters using DFT[66] and observed in dioxygen metal complexes.[33]

For completion, we mention the adsorption over the fcc site (E) depicted in Figure 4. The molecule is slightly inclined with respect to the local surface plane of the {111} microfacet. The molecule is tilted by 11.5° toward the bridge site on the ridge, and the molecular center of mass is displaced 0.18 Å away from the "ideal" fcc position, toward the second-layer top site. The corresponding O−O bond length is 1.41 Å, and the adsorbate center of mass is located at a height of 1.73 Å above the microfacet surface plane. The relaxed adsorbate structure closely resembles that calculated for adsorption in the equivalent site on the Pt{111} surface, for which an O−O bond length, tilt angle, and adsorbate height of 1.43 Å, 10.1°, and 1.78 Å was determined by Eichler et al.[39,40] with values of 1.39 Å, 10.7°, and 1.83 Å being obtained by Bocquet et al.[65]

V. Electronic Structure Analysis

The electronic and magnetic properties of the chemisorbed molecular species may be characterized by considering both the change in the charge density distribution on adsorption and by analyzing the calculated total charge density of the system using the Bader topological model.[54,55] In the latter case, characteristic topological features of the total charge density are used to partition the density into regions attributable to each atom in the system, from which the corresponding atom-resolved charge and magnetic moment may be obtained.

TABLE 3: Atom-resolved Charges, *q*, and Magnetic Moments, μ, for the Six Lowest-Energy Adsorption Sites of O_2 on Pt{110}(1 × 2)[a]

site	A[d]	A′[d]	E	G	K	L	H
q_{Pt}[b]	0.45	0.46	0.57	0.46	0.51	0.51	0.52
q_{O_2}[c]	−0.54	−0.55	−0.69	−0.54	−0.51	−0.48	−0.52
μ_{O_2}[c]	0.42	0.00	0.00	0.56	0.02	0.71	0.57

[a] Units are the electronic charge, e, and Bohr magneton, μ_B, respectively. [b] q_{Pt} is the combined charge on the Pt substrate atoms directly involved in the adsorbate bond. [c] q_{O_2} and μ_{O_2} are the total charge and magnetic moment of the oxygen molecule, respectively. [d] A and A′ represent two energetically degenerate electronic minima for adsorption in the ridge-bridge site, obtained using different density mixing parameters.

A. Charge and Magnetization. The results of the Bader analysis for the six lowest-energy sites for molecular oxygen adsorption on Pt{110}(1 × 2) are summarized in Table 3. For all sites, the calculated net electron flow is from the Pt substrate to the O_2 adsorbate, so that the molecule acquires a net negative charge. This is consistent with the increase in work function observed for O_2 adsorption on this surface,[23,24] although in general the limitations of directly equating a net negative charge on the adsorbate with an increase in work function should be noted.[67] From Table 3, it is apparent that the most negatively charged species corresponds to adsorption over the fcc hollow site (E), resulting in a net charge of −0.69 e on the molecule and simultaneous quenching of the molecular magnetic moment. In contrast, the lowest electron transfer, −0.48 e, is observed for adsorption in the long-bridge site (L), for which the least reduction in the molecular magnetic moment is obtained. The net charge accumulated on the O_2 admolecule for the three bridge sites (A, G, and H) is very similar, reflecting the similarity of the adsorption site and the nature of the interaction of the adsorbate with the substrate. However, in the case of the rotated long-bridge site (K), the calculated results seem almost anomalous, with a comparatively low electron transfer of −0.51 e accompanying a complete quenching of the molecular spin. Thus, it does not appear to be possible to equate the absolute charge transfer to the O_2 molecule with the reduction in the molecular spin moment. The charge on the admolecule is, for example, almost identical for adsorption in both the rotated long-bridge site (K), −0.51 e, and second-layer bridge site (H), −0.52 e, but in the former case, the molecular spin-polarization is reduced to zero, while in the latter case, a magnetic moment of $0.57\mu_B$ is retained on the molecule.

From Table 3, it is also apparent that a significant portion of the charge acquired by the adsorbed molecule originates from the Pt substrate atoms directly coordinated to the admolecule. Thus, for short (A, G, H) and long (K, L) bridge sites, the charge predominantly flows from the bridge Pt atoms to which the O_2 molecule is coordinated, while for the hollow site (E) the combined reduction in charge on the three Pt atoms of the fcc site, 0.57 e, accounts for the majority of the negative charge accumulated on O_2 (−0.67 e).

The neutral gas-phase oxygen molecule has two partially occupied antibonding $1\pi_g^*$ orbitals. Donation of one or two electrons into these orbitals results in a superoxide (O_2^-) or peroxide (O_2^{2-}) ion, respectively. The increase in the number of antibonding electrons leads to an increase in the bond length and a concomitant decrease in the O−O stretching frequency relative to that of the neutral molecule. A clear and unambiguous distinction between the superoxide ion and peroxide ion can therefore be made.

Molecular oxygen chemisorbed on a metal surface may similarly be classified as superoxo-like or peroxo-like. In this case, however, there is no unique definition of the two types of species. In the case of O_2 adsorption on Pt{110}(1 × 2), for example, EELS results[31,32] were interpreted in terms of peroxo-like and superoxo-like species on the surface. The lower frequency losses observed by Schmidt et al.[32] at 860 and 930 cm^{-1} were assigned to peroxo-like oxygen, while an additional loss at 1250 cm^{-1} observed at high coverage and low temperature (T < 100 K) was attributed to superoxo-like oxygen. In this case, the superoxo/peroxo classification was based solely on the observed stretching frequencies of the species, compared with those observed for peroxide and superoxide ions and in dioxygen metal complexes.[33]

The superoxide and peroxide ions are also characterized by the donation of electrons into one or both of the partially filled $1\pi_g^*$ orbitals. A nonzero magnetic moment is therefore retained on the superoxide ion (O_2^-), but the magnetic moment is reduced to zero for the peroxide ion (O_2^{2-}). Thus, an alternative superoxo/peroxo classification scheme for chemisorbed oxygen may be based on whether one or both of the molecular $1\pi_g^*$ orbitals are filled upon formation of the adsorbate−metal bond, with a concomitant retention or quenching of the molecular magnetic moment, respectively. Within this definition, peroxo-like and superoxo-like chemisorbed species have been identified on Pt{111} using NEXAFS.[36−38] It is important to note, however, that the two different classification schemes, the first based on the observed stretching frequencies and the second on the number of $1\pi_g^*$ orbitals implicated in the adsorbate−metal bond, are not necessarily consistent with each other. Thus, a species classified as peroxo-like in one scheme may be termed superoxo-like in another.

In the present study, the calculated magnetic moments for the adsorbed O_2 species, μ_{O2}, given in Table 3 are used to classify the admolecules as peroxo-like or superoxo-like, within the second definition described above. In this case, complete quenching of the molecular magnetic moment is attributed to filling of both $1\pi_g^*$ orbitals on bonding and hence is associated with peroxo-like oxygen. Donation only into the $1\pi_g^*$ orbital orientated perpendicular to the surface (refer to section VB) results in a partial quenching of μ_{O2} and characterizes superoxo-like oxygen. The results in Table 3 indicate that the species adsorbed in the fcc hollow site (E) and in the long-bridge site with the rotated configuration (K) may be characterized as peroxo-like species, since for these sites the magnetic moment is reduced to zero upon adsorption. The species adsorbed in sites G, L, and H may be classified as superoxo-like, retaining a magnetic moment of between $0.56\mu_B$ and $0.71\mu_B$, depending on the adsorption site.

The spin character of oxygen adsorbed in the lowest-energy adsorption site, the bridge site on the ridge (site A), deserves special mention. Initial calculation of the adsorption of O_2 in this site resulted in a superoxo-like chemisorbed molecular species with a magnetic moment of $0.42\mu_B$ (A in Table 3). However, in a separate calculation, a peroxo-like species, energetically degenerate with the former superoxo species (to within 0.03 eV) but with zero magnetic moment, was obtained (A′ in Table 3). The two calculations differed *only* in terms of the parameters controlling the density mixing history and amplitude. Both calculations were started with the same initial geometry and with a zero spin configuration (equal number of up and down spin electrons). In the case of the calculation yielding the zero spin species, a longer mixing history and smaller mixing amplitude were used. The longer mixing history may explain the tendency for the electronic configuration to remain in the initial zero spin configuration. The density mixing parameters do not, however, affect the validity of the final electronic configuration, only changing the "route" to the self-consistent solution.[68] It is not clear if the peroxo and superoxo solutions are both physically valid or if the approximate nature of the exchange-correlation energy functional results in an inability of the density functional approach to distinguish energetically between the two possibilities. The adsorption geometry calculated for the peroxo-like O_2 molecule is identical to that found for the superoxo-like species illustrated in Figure 2, to within 0.01 Å. The net charge flow from the substrate to adsorbate is also similar, with calculated values of −0.55 e on O_2 and 0.46 e on the bridge Pt atoms (A′ in Table 3) as opposed to the superoxo species for which values of −0.54 e and 0.45 e were obtained, respectively (A in Table 3).

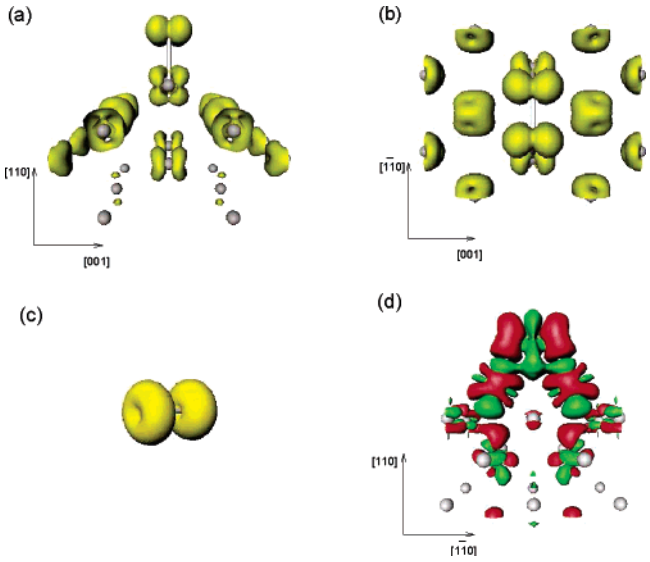

Figure 5. Isosurfaces of the spin-density for O_2 adsorbed in the bridge site along the Pt ridge, corresponding to a spin-density of 5.7×10^{-2} electrons/Å^3, viewed down the close-packed ridge in the [1$\bar{1}$0] direction (a) and from above the {110} plane (b). (c) Spin-density of an isolated O_2 molecule. (d) Isosurfaces of the difference electron density for adsorption in the same site. Red (dark) contours represent an electron density increase of 1.7×10^{-2} electrons/Å^3; green (light) contours indicate a decrease by 1.7×10^{-2} electrons/Å^3. The [110] direction is normal to the surface, the [001] direction is across the troughs, and the [1$\bar{1}$0] direction is along the close-packed rows.

B. Bonding Characterization. The nature of the bonding interaction between the adsorbed O_2 molecule and the Pt substrate may be characterized by examining isosurfaces of the spin-density $\rho_\alpha(\mathbf{r}) - \rho_\beta(\mathbf{r})$, where $\rho_\alpha(\mathbf{r})$ and $\rho_\beta(\mathbf{r})$ are the majority and minority spin densities, respectively, as well as isosurfaces of the difference electron density. In the latter case, the charge density is determined for the adsorbate system and then for the Pt substrate and the O_2 molecule alone, each in the optimized geometry obtained for the combined system. The difference between the charge density distribution of the adsorption system and the sum of the distributions for the Pt substrate and O_2 adsorbate, $\rho(\text{slab} + O_2) - \rho(\text{slab}) - \rho(O_2)$, reveals the redistribution of the charge upon adsorption.

Isosurfaces of the spin-density of O_2 adsorbed in the lowest-energy adsorption site, the bridge site on the Pt ridge, are illustrated in parts a and b of Figure 5, with that of the isolated gas-phase O_2 molecule shown in Figure 5c for comparison. The difference electron density for this site is illustrated in Figure 5d. Here, we concentrate the discussion on the superoxo-like species described above. The spin-density distribution for the

isolated O_2 molecule shown in Figure 5c arises from the set of two $1\pi_g^*$ molecular orbitals which are orientated perpendicular to each other and which are both partially occupied. Upon adsorption, the charge flow to the molecule appears to result in a preferential occupation of states arising from the π_g^* orbital orientated perpendicular to the surface, so that a nonzero spin-density is retained on the O_2 molecule only in the orbital aligned parallel to the surface. There is an induced magnetization of d_{xz} symmetry on the ridge Pt atoms, with further spin character present on both the second- and third-layer Pt atoms. The induced magnetization on the second and third substrate layers is borne out by the Bader analysis discussed in section VA, from which it is found that the induced magnetization is only reduced to negligible values for the atoms of the fourth layer. It should be noted, however, that the top three Pt layers are under-coordinated with respect to the bulk coordination and, in this sense, may be considered to be surface atoms. Furthermore, with the exception of the third-layer trough atoms below the missing row, all the Pt substrate atoms for which an induced magnetization is present are nearest-neighbors of the ridge atoms to which the O_2 molecule is directly bonded. In this context, the extent of the magnetization of the Pt substrate induced on adsorption of O_2 seems reasonable.

Isosurfaces of the difference electron density illustrated in Figure 5d suggest that the adsorbate molecular orbitals interact predominantly with the substrate d-orbitals, resulting in a redistribution of the charge density due to these states. Charge is donated both to and from O_2, indicated by the red (dark) and green (light) isodensity surfaces on the molecule in Figure 5d, respectively. However, electron donation to the molecule clearly dominates, since from the Bader analysis a net negative charge of -0.54 e is accumulated on the admolecule (Table 3).

VI. Conclusions

The adsorption of molecular oxygen on the Pt{110}(1×2) surface has been investigated using calculations based on spin-DFT. A strong energetic preference for adsorption in the ridge-bridge site is found, with the molecular axis aligned along the close-packed rows. The corresponding chemisorption energy and O−O vibrational stretching frequency calculated for this site are -1.48 eV/molecule and 877 cm^{-1}, respectively. Adsorption in the ridge-bridge site is favored by at least 0.56 eV/molecule over all other sites considered in this study. On the basis of our results, in combination with previous NEXAFS[22,26] and EELS[31,32] studies, we conclude that the ridge-bridge site is populated first. At higher coverages, we suggest that the long-bridge site in the valley of the reconstructed surface is occupied, although without entirely excluding the possibility of adsorption in the bridge sites located on the {111} microfacets.

Acknowledgment. We acknowledge financial support for this work from the EPSRC (U.K.), in the form of funds for workstations. M.A.P. thanks the Oppenheimer Trust for a research studentship and the Cambridge Commonwealth Trust for financial assistance. S.J.J. thanks The Royal Society for a University Research Fellowship. Additional resources were provided by the Cambridge-Cranfield High Performance Computing Facility.

References and Notes

(1) Li, W. X.; Osterlund, L.; Vestergaard, E. K.; Vang, R. T.; Matthiesen, J.; Pedersen, T. M.; Lægsgaard, E.; Hammer, B.; Besenbacher, F. *Phys. Rev. Lett.* **2004**, *93*, 146104.

(2) Li, W. X.; Stampfl, C.; Scheffler, M. *Phys. Rev. Lett.* **2003**, *90*, 256102.

(3) Reuter, K.; Scheffler, M. *Appl. Phys. A* **2004**, *78*, 793.

(4) Hou, Y. C.; Jenkins, S. J.; King, D. A. *Surf. Sci. Lett.* **2004**, *550*, L27.

(5) Kellogg, G. L. *Phys. Rev. Lett.* **1985**, *55*, 2168.

(6) Sowa, E. C.; van Hove, M. A.; Adams, D. L. *Surf. Sci.* **1988**, *199*, 174.

(7) Fery, P.; Moritz, W.; Wolf, D. *Phys. Rev. B* **1988**, *38*, 7275.

(8) Jenkins, S. J.; Petersen, M. A.; King, D. A. *Surf. Sci.* **2001**, *494*, 159.

(9) Walker, A. V.; Klötzer, B.; King, D. A. *J. Chem. Phys.* **1998**, *109*, 6879.

(10) Hickman, D. A.; Schmidt, L. D. *Science* **1993**, *259*, 343.

(11) Walker, A. V.; King, D. A. *J. Chem. Phys.* **2000**, *112*, 1937.

(12) Walker, A. V.; King, D. A. *Phys. Rev. Lett.* **1999**, *82*, 5156.

(13) Walker, A. V.; King, D. A. *J. Chem. Phys.* **2000**, *112*, 4739.

(14) Walker, A. V.; King, D. A. *J. Phys. Chem. B* **2000**, *104*, 6462.

(15) Walker, A. V.; King, D. A. *Surf. Sci.* **2000**, *444*, 1.

(16) Watson, D. T. P.; Titmuss, S.; King, D. A. *Surf. Sci.* **2002**, *505*, 49.

(17) Watson, D. T. P.; van Dijk, J.; Harris, J. J. W.; King, D. A. *Surf. Sci.* **2002**, *506*, 243.

(18) Watson, D. T. P.; Harris, J. J. W.; King, D. A. *Surf. Sci.* **2002**, *505*, 58.

(19) Watson, D. T. P.; Harris, J. J. W.; King, D. A. *J. Phys. Chem. B* **2002**, *106*, 3416.

(20) Horch, S.; Lorensen, H. T.; Helveg, S.; Lægsgaard, E.; Stensgaard, I.; Jacobsen, K. W.; Nørskov, J. K.; Besenbacher, F. *Nature* **1999**, *398*, 134.

(21) Ohno, Y.; Matsushima, T. *Surf. Sci.* **1991**, *241*, 47.

(22) Ohno, Y.; Matsushima, T.; Tananka, S.; Kamada, M. *Jpn. J. Appl. Phys.* **1993**, Suppl. 32-2, 383.

(23) Fusy, J.; Ducros, R. *Surf. Sci.* **1989**, *214*, 337.

(24) Freyer, N.; Kiskinova, M.; Pirug, G.; Bonzel, H. *Surf. Sci.* **1986**, *166*, 206.

(25) Prince, K. C.; Dückers, K.; Horn, K.; Cháb, V. *Surf. Sci.* **1988**, *200*, L451.

(26) Ohno, Y.; Matsushima, T.; Tananka, S.; Yagasaki, E.; Kamada, M. *Surf. Sci.* **1992**, *275*, 281.

(27) Ducros, R.; Fusy, J. *Appl. Surf. Sci.* **1990**, *44*, 59.

(28) Dückers, K.; Prince, K. C.; Bonzel, H. P.; Cháb, V.; Horn, K. *Phys. Rev. B* **1987**, *36*, 6292.

(29) Ducros, R.; Ehrhardt, J. J.; Fusy, J.; Mutaftschiev, B. *Phys. Rev. B* **1988**, *38*, 10035.

(30) Silva, J. L. F. D.; Stampfl, C.; Scheffler, M. *Phys. Rev. Lett.* **2003**, *90*, 066104.

(31) Sobyanin, V. A.; Zamaraev, K. I. *React. Kinet. Catal. Lett.* **1986**, *31*, 273.

(32) Schmidt, J.; Stuhlmann, C.; Ibach, H. *Surf. Sci.* **1993**, *284*, 121.

(33) Vaska, L. *Acc. Chem. Res.* **1976**, *9*, 175.

(34) Gland, J. L.; Sexton, B. A.; Fisher, G. B. *Surf. Sci.* **1980**, *95*, 587.

(35) Steininger, H.; Lehwald, S.; Ibach, H. *Surf. Sci.* **1982**, *123*, 1.

(36) Outka, D. A.; Stöhr, J.; Jark, W.; Stevens, P.; Solomon, J.; Madix, R. J. *Phys. Rev. B* **1987**, *35*, 4119.

(37) Wurth, W.; Stöhr, J.; Feulner, P.; Pan, X.; Bauchspiess, K. R.; Baba, Y.; Hudel, E.; Rocker, G.; Menzel, D. *Phys. Rev. Lett.* **1990**, *65*, 2426.

(38) Puglia, C.; Nilsson, A.; Hernnäs, B.; Karis, O.; Bennich, P.; Mårtensson, N. *Surf. Sci.* **1995**, *342*, 119.

(39) Eichler, A.; Hafner, J. *Phys. Rev. Lett.* **1997**, *79*, 4481.

(40) Eichler, A.; Mittendorfer, F.; Hafner, J. *Phys. Rev. B* **2000**, *62*, 4744.

(41) Panas, I.; Siegbahn, P. *Chem. Phys. Lett.* **1988**, *153*, 458.

(42) Ferrer, S.; Bonzel, H. P. *Surf. Sci.* **1982**, *119*, 234.

(43) Wilf, M.; Dawson, P. T. *Surf. Sci.* **1977**, *65*, 399.

(44) Payne, M. C.; Teter, M. P.; Allan, D. C.; Arias, T. A.; Joannopoulos, J. D. 1992, CASTEP 3.9 academic version, licensed under the UKCP-MSI Agreement, 1999.

(45) Perdew, J. P.; Chevary, J. A.; Vosko, S. H.; Jackson, K. A.; Pederson, M. R.; Singh, D. J.; Fiolhais, C. *Phys. Rev. B* **1992**, *46*, 6671.

(46) Vanderbilt, D. *Phys. Rev. B* **1990**, *41*, 7892.

(47) Lide, D. R., Ed. In *Handbook of Chemistry and Physics*, 75th ed.; CRC Press LCC: New York, 1998.

(48) Monkhorst, H. J.; Pack, J. D. *Phys. Rev. B* **1976**, *13*, 5188.

(49) Gillan, M. J. *J. Phys.: Condens. Matter* **1989**, *1*, 689.

(50) DeVita, A.; Gillan, M. *J. Phys.: Condens. Matter* **1991**, *3*, 6225.

(51) Petersen, M. A.; Watson, D. T. P.; Jenkins, S. J.; King, D. A. *J. Chem. Phys.* **2002**, *117*, 3951.

(52) Petersen, M. A.; Jenkins, S. J.; King, D. A. *J. Phys. Chem. B* **2004**, *108*, 5909.

(53) Petersen, M. A.; Jenkins, S. J.; King, D. A. *J. Phys. Chem. B* **2004**, *108*, 5920.

(54) Bader, R. W. F. *Atoms in Molecules: A Quantum Theory*; Oxford University Press: Oxford, U.K., 1990.

(55) Popelier, P. *Atoms in Molecules: An Introduction*; Pearson Education: Harlow, U.K., 2000.

(56) Yamagishi, S.; Jenkins, S. J.; King, D. A. *J. Am. Chem. Soc.* **2004**, *126*, 10962.

(57) Yamagishi, S.; Jenkins, S. J.; King, D. A. *Surf. Sci.* **2003**, *543*, 12.

(58) Yamagishi, S.; Jenkins, S. J.; King, D. A. *Chem. Phys. Lett.* **2003**, *367*, 116.

(59) Yamagishi, S.; Jenkins, S. J.; King, D. A. *J. Chem. Phys.* **2002**, *117*, 819.

(60) Yamagishi, S.; Jenkins, S. J.; King, D. A. *J. Chem. Phys.* **2001**, *114*, 5765.

(61) Held, G.; Braun, W.; Steinrück, H. P.; Yamagishi, S.; Jenkins, S. J.; King, D. A. *Phys. Rev. Lett.* **2001**, *87*, 216102.

(62) Jenkins, S. J.; Ge, Q.; King, D. A. *Phys. Rev. B* **2001**, *64*, 012413.

(63) Ge, Q.; Jenkins, S. J.; King, D. A. *Chem. Phys. Lett.* **2000**, *327*, 125.

(64) Panchenko, A.; Koper, M. T. M.; Shubina, T. E.; Mitchell, S. J.; Roduner, E. *J. Electrochem. Soc.* **2004**, *151*, A2016.

(65) Bocquet, M. L.; Cerdà, J.; Sautet, P. *Phys. Rev. B* **1999**, *59*, 15437.

(66) Li, T.; Balbuena, P. *J. Phys. Chem. B* **2001**, *105*, 9943.

(67) Michaelides, A.; Hu, P.; Lee, M. H.; Alavi, A.; King, D. A. *Phys. Rev. Lett.* **2003**, *90*, 246103.

(68) For the remaining adsorption sites considered, the possibility of finding metastable states with a different spin configuration cannot be excluded. However, it is likely that such metastable states would be significantly higher in energy than the energetic minima we have located, particularly for metastable states with higher spin configurations than those reported here. There is no a priori reason to expect that the energetic degeneracy of the superoxo and peroxo states found for the ridge-bridge geometry should occur for any of the other adsorption geometries considered. We note that all spin-polarized calculations reported here were started with an equal number of spin-up and spin-down electrons, corresponding to an initial zero spin-polarization at the start of the calculation.